

Electronic Structures and Phonon Spectra in Boronitride Superconductors $\text{La}\mathcal{M}\text{BN}$ ($\mathcal{M} = \text{Ni, Pt}$)

Myung-Chul Jung¹, Chang-Jong Kang², B. I. Min², and Kwan-Woo Lee^{1,3*}

¹Department of Applied Physics, Graduate School, Korea University, Sejong 339-700, Korea

²Department of Physics, PCTP, Pohang University of Science and Technology, Pohang 790-784, Korea

³Department of Display and Semiconductor Physics, Korea University, Sejong 339-700, Korea

(Dated: August 15, 2018)

We have investigated electronic structures and phonon spectra of newly discovered isostructural superconductors LaNiBN ($T_c = 4.1$ K) and LaPtBN ($T_c = 6.7$ K). We have found that their electronic structures are substantially three-dimensional, leading to metallicity both in NiB (PtB) and the intervening LaN layers. Our *ab initio* phonon calculations show that almost all phonon modes contribute to the electron-phonon coupling (EPC) mechanism, reflecting that both layers are involved in the superconductivity. For LaNiBN , we obtain an EPC strength of $\lambda = 0.52$ and a logarithmically averaged characteristic phonon frequency of $\omega_{\log} = 376$ K, leading to $T_c = 3.9$ K. Compared with the Ni B_{1g} mode in LaNiBN , the Pt B_{1g} mode in LaPtBN is reduced by $\sim 70\%$, leading to a slightly enhanced $\lambda = 0.56$ and an $\sim 20\%$ reduced ω_{\log} . The estimated T_c is 5.4 K for LaPtBN , in good agreement with the experiment. We do not find any indication of magnetic instability for either LaNiBN or LaPtBN , which implies that both systems are EPC mediated superconductors. Further, we have found an interesting trend of monotonic increase of T_c with respect to the boron height in the NiB (PtB) layer of both borocarbide and boronitride superconductors, which suggests a possible way to enhance T_c in these systems.

PACS numbers: 71.20.Be, 74.70.Dd, 74.25.Kc, 71.20.Lp

I. INTRODUCTION

After the discovery of high- T_c superconductors in cuprates and, more recently, in Fe pnictides, layered systems containing transition metals (TMs), which in particular form a square lattice, have been extensively studied. These systems are of extreme interest due to their potential for being high- T_c superconductors induced by the interplay between superconductivity and magnetic fluctuation. In this point of view, boronitrides of $(\text{LaN})_n(\mathcal{M}_2\text{B}_2)$ (n = number of layers, \mathcal{M} = TM) and borocarbides of $(\mathcal{RC})_n(\mathcal{M}_2\text{B}_2)$ (\mathcal{R} = rare-earth element), which exhibit various intriguing physical phenomena related to superconductivity and magnetism, have attracted immense attention.^{1,2} In this research, we will focus on $n = 2$ boronitride superconductors LaNiBN and LaPtBN , recently discovered by Imamura *et al.*,³ in order to understand the nature of their superconductivity.

About 20 years ago, Cava *et al.* observed superconductivity in $n = 3$ boronitride $\text{La}_3\text{Ni}_2\text{B}_2\text{N}_3$ at $T_c = 13$ K.⁴ They synthesized $n = 2$ boronitride LaNiBN too but failed to observe the superconductivity above 4.2 K. LaNiBN showed ten times higher resistivity than the normal-state $\text{La}_3\text{Ni}_2\text{B}_2\text{N}_3$.⁴ Very recently, Imamura *et al.* successfully prepared a bulk superconducting LaNiBN sample with $T_c = 4.1$ K, using a technique involving a high temperature of 1200 °C and a high pressure of 5 GPa.³ Two isostructural superconducting compounds, LaPtBN and CaNiBN , were also synthesized with $T_c = 6.7$ and 2.2 K, respectively.³

These boronitrides show some distinctions as well as similarities in crystal structure compared to Fe pnictides. These systems commonly have inverse α - PbO -type \mathcal{M} -B

layers, but in the $n = 2$ boronitrides \mathcal{M} -B layers are separated by two LaN layers with a width of $2.5 (\pm 0.1)$ Å, as displayed in Fig. 1. As will be addressed below, boronitrides have metallic $(\text{LaN})^0$ intervening layers, while a superconducting Fe pnictide, LaFeAsO , possesses insulating $(\text{LaO})^{1+}$ intervening layers.

In the Ni-based borocarbides, which are isostructural with boronitrides, the interplay between superconductivity and magnetic fluctuation has been extensively discussed.^{1,2} Pt-based superconductors often show unconventional superconductivity due to large spin-orbital coupling (SOC), incipient magnetism, and multi-gap nature.⁵⁻¹¹ Superconducting CePt_3Si and $\text{Li}_2\text{Pt}_3\text{B}$, which do not have inversion symmetry, show significant SOC, possibly leading to the exotic superconductivity.⁶⁻⁸ On the other hand, the effects of SOC in superconducting SrPt_3P are negligible.⁹ So it is of interest to clarify whether the effects of SOC or magnetism matter in LaNiBN and LaPtBN . However, except for the observation of superconductivity, other data in the literature are still very limited.

In this paper, we will address the electronic structures, including fermiology, which indicate no magnetic instability and negligible SOC effects in both superconducting boronitrides. Then, the phonon spectra and the electron-phonon coupling (EPC) will be discussed to unveil the mechanism of the superconductivity.

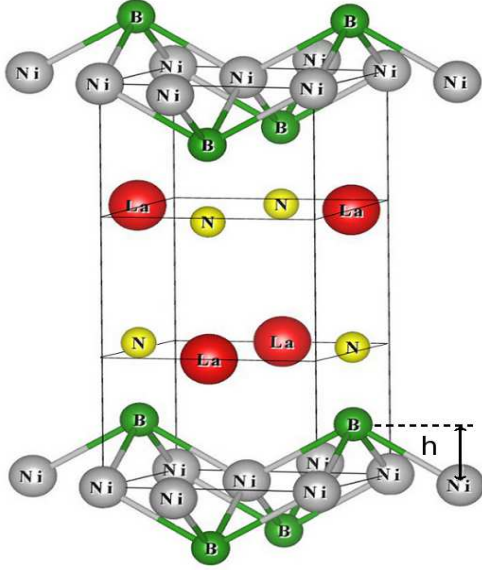


FIG. 1: (Color online) Crystal structure of LaMBN , which contains two formula units in the primitive cell. The inverse $\alpha\text{-PbO}$ -type MB layers are separated by two LaN layers. In our relaxed structure, the Ni-B and Pt-B bond lengths are 2.17 and 2.30 Å, respectively. The M-B-M bond angles are 74.8° in LaNiBN and 71.9° in LaPtBN . The symbol h indicates the boron height in the M-B layer.

II. STRUCTURE AND CALCULATION METHOD

In the tetragonal structure of LaMBN (space group: $P4/nmm$, No. 129), as shown in Fig. 1, the M atoms lie on the $2b$ sites ($\frac{3}{4}, \frac{1}{4}, \frac{1}{2}$), while the other atoms sit at the $2c$ sites ($\frac{3}{4}, \frac{3}{4}, z$). Our calculations were carried out with the experimental lattice constants: $a = 3.73$ Å and $c = 7.64$ Å for LaNiBN and $a = 3.8240$ Å and $c = 7.8649$ Å for LaPtBN .^{3,15} These values lead to an 8% larger volume in LaPtBN , consistent with the larger atomic radius of Pt. The internal parameters z were optimized using an accurate all-electron full-potential code (FPLO)¹³ because of the inaccuracy of the initial experimental data in LaNiBN discussed earlier¹² and the lack of available data for LaPtBN . The optimized values show tiny differences of at most 0.02 Å between the local-density approximation (LDA) and the Perdew-Burke-Ernzerhof (PBE) generalized gradient approximation (GGA),¹⁴ indicating that these values are nearly independent of the exchange-correlation functional. In LaNiBN , the optimized values z are 0.1770 for La, 0.3545 for B, and 0.1636 for N. The corresponding z values of LaPtBN are 0.1666 for La, 0.3366 for B, and 0.1527 for N. The differences in z between the experimental and our relaxed values are substantial, 0.65 Å for B and 0.13 Å for N,¹⁵ but they are consistent with the relaxed values by Singh and Pickett for $\text{La}_3\text{Ni}_2\text{B}_2\text{N}$,¹⁶ showing differences of 0.45 Å for B and 0.10 Å for N. Using our optimized values, the B-N

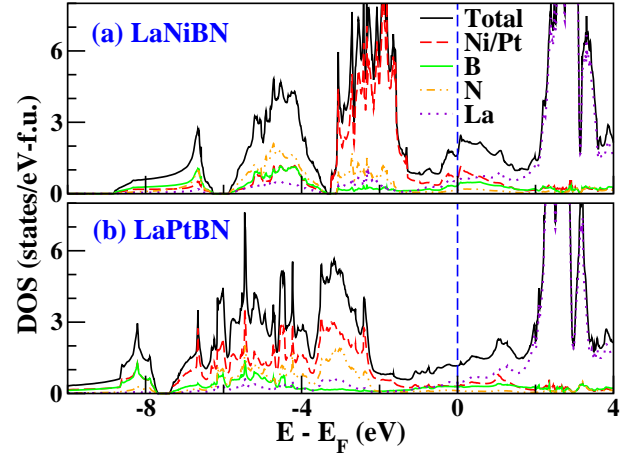


FIG. 2: (Color online) Total and atom-projected densities of states (DOSs) of LaNiBN and LaPtBN . LaPtBN has 30% smaller DOS $N(E_F)$ at the Fermi energy E_F than LaNiBN . $N(E_F)$'s are decomposed into roughly 40% Ni, 30% La, 20% B, and 10% N for LaNiBN and into approximately 26% Pt, 40% La, 24% B, and 10% N for LaPtBN . Both systems have a van Hove singularity at ~ 80 meV, suggesting to enhance T_c by small amount of electron doping.

bond lengths of $1.45 (\pm 0.01)$ Å are obtained for both systems, which are in agreement with the optimized values in the pseudopotential code CASTEP by Imamura *et al.*,³ whereas the M-B bond length is 6% longer in LaPtBN . These indicate that our optimized values are well converged. In addition, by reducing the volume by 5%, the B-N bond length remains unchanged, implying strong B-N bonding and stiffness of the lattice (see below). The structural parameters were optimized until forces were smaller than 1 meV/Å.

For the full phonon calculations, we used the linear response method within the GGA implemented in the QUANTUM ESPRESSO package,¹⁷ which produces optimized internal parameters very close to those of FPLO. Our phonon calculations were carried out with the PBE ultrasoft pseudopotentials, a Gaussian smearing factor of 0.05 Ry, a wave-function cutoff of 40 Ry, and a charge cutoff of 400 Ry. We used a $14 \times 14 \times 14$ k mesh and a $2 \times 2 \times 2$ q mesh for the phonon calculations and a $28 \times 28 \times 28$ k mesh for the EPC calculations, which require more careful treatment of the Fermi energy E_F .

III. ELECTRONIC STRUCTURES

A. Magnetic tendencies

First, we address whether a magnetic instability is feasible in these boronitrides. Fig. 2 shows the total and atom-projected densities of states (DOSs) for both systems. DOSs at E_F , $N(E_F)$, are seen to be rather low, 1.65 and 1.17 (in units of states per eV per formula unit), which is consistent with the bad metallic character ob-

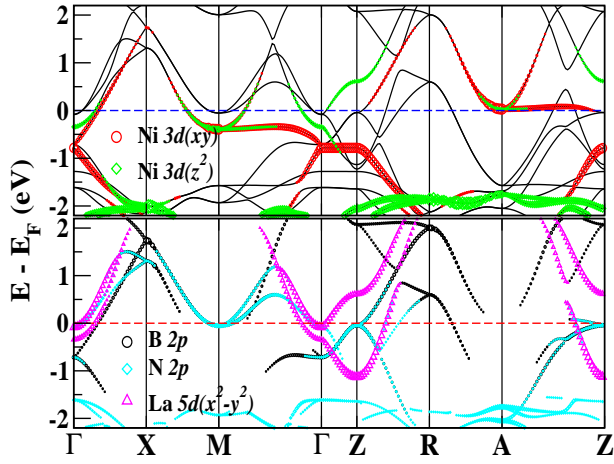


FIG. 3: (Color online) (top) Nonmagnetic band structure with Ni $3d_{xy}$ and $3d_{z^2}$ fat bands of LaNiBN in the optimized structure. (bottom) Fat bands of B $2p$, N $2p$, and La $5d_{x^2-y^2}$ orbitals, clearly indicating substantial B-N hybridization and a metallic LaN layer. The horizontal dashed lines denote E_F . The symmetry points are $\Gamma(Z) = (0,0,\xi)$, $X(R) = (1,0,\xi)$, and $M(A) = (1,1,\xi)$ in units of $(a/\pi, a/\pi, c/\pi)$. Here, ξ is 0 for the first symbols and 1 for the symbols in parentheses.

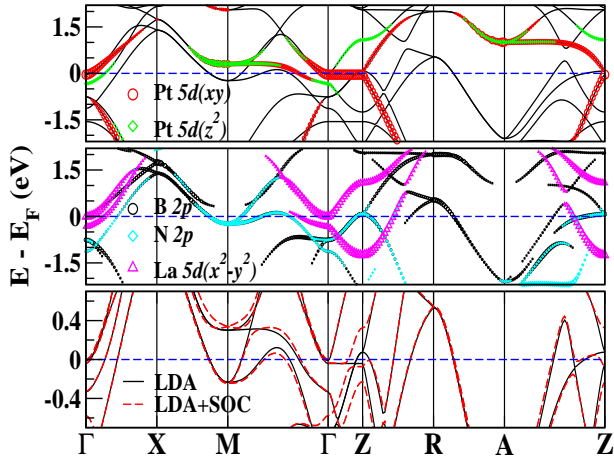


FIG. 4: (Color online) (top) Nonmagnetic band structure with Pt $5d_{xy}$ and $5d_{z^2}$ fat bands of LaPtBN in the optimized structure. (middle) Fat bands of B $2p$, N $2p$, and La $5d_{x^2-y^2}$ orbitals. (bottom) Overlapped LDA and LDA + SOC band structures in the range of -0.7 to 0.87 eV, showing some distinctions along the Γ -Z line just below E_F and at the M point above E_F but leading to negligible effects on the superconductivity (see text).

served in their normal states. These values lead to bare specific-heat coefficients of 3.9 and 2.8 mJ/mol-K² for LaNiBN and LaPtBN, respectively, which are approximately a quarter of that of Fe pnictides in the nonmagnetic state. In contrast to the Fe pnictides, this implies less magnetic instability, or lack of magnetic instability, in these boronitrides. Additionally, the contribution of Ni

to $N(E_F)$ is small, 0.33 states/eV-spin-f.u. for LaNiBN. The contribution of Pt in LaPtBN is only half of this value. Using a typical intra-atomic exchange parameter of Ni $I \approx 1$ eV,¹⁸ the Stoner factor $IN(E_F)$ is estimated to be 0.33 for LaNiBN, which is much smaller than unity. So neither metamagnetism nor a near-stable ferromagnetic state is indicated. This feature is confirmed also by our fixed spin moment calculations in both systems (not shown here). Again, no stable (anti)ferromagnetic states can be obtained from our calculations of both the local spin-density approximation and GGA for both systems.

Interestingly, considering a partial contribution of each atom at E_F , $N(E_F)$ of La₃Ni₂B₂N₃ can be exactly reproduced from that of LaNiBN. This may imply a common mechanism of the superconductivity in both systems. Note that La₃Ni₂B₂N₃ has higher T_c by a factor of 3 and larger DOS at E_F in the unit cell by a factor of $\frac{3}{2}$ than LaNiBN.¹⁶

B. Nonmagnetic electronic structures

Now, we will focus on the nonmagnetic states, which represent the superconducting state. For LaNiBN, as shown in the DOS in Fig. 2(a), Ni $3d$ states mainly lie in the range of -3.5 to -1 eV. Below that regime, two separated manifolds have nearly equally mixed characters of B, N, and Ni ions but relatively small La character. Near E_F , the characters of all atoms appear, indicating metallicity in both NiB and LaN layers, as observed in La₃Ni₂B₂N₃.¹⁶ The Fermi energy pinpoints the midway of two small peaks, resulting from the dispersionless bands with the mixed Ni $3d_{xy}$ and $3d_{z^2}$ characters along the M - Γ line at -0.5 eV and along the A - Z line at 50 meV, as displayed in Fig. 3. In many regimes near E_F , a mixture of these partially filled orbitals appears, reflecting strong hybridization between inter- and intra layers. The bottom panel of Fig. 3 obviously indicates the metallic La $5d_{x^2-y^2}$ band.

The total and atom-projected DOSs of the $5d$ counterpart LaPtBN are given in Fig. 2(b). As expected, the main part of Pt $5d$ orbitals is more widely spread over the range of -7.5 to -2 eV, but some tail extends to 2 eV. The total DOS smoothly increases near E_F , except for a van Hove singularity at 80 meV, suggesting less sensitivity to carrier doping or moderate pressure. The corresponding band structure and fat bands of the partially filled orbitals are plotted together in Fig. 4. A comparison with those of LaNiBN shows some distinctions in several regimes, in particular, around the M point and along the Γ -Z and the A -Z lines. At the M point degenerate bands of B and N $2p$ orbitals move below E_F . To compensate for this, the two fold degenerate flat bands with Pt $5d_{xy}$ and $5d_{z^2}$ orbital character shift up, being unfilled at the M and A points. These bands are reflected as small peaks at 0.3 and 1 eV in the DOS in Fig. 2(b). A more pronounced feature is the flat Pt $5d_{xy}$ band lying at -40 meV along the Γ -Z line, while the

corresponding Ni band exists at -1 eV in LaNiBN. This leads to some differences in the phonon spectra, which will be addressed below.

These distinctions are also analyzed through interpretation of the occupation matrix, which is useful for understanding the oxidation state.¹⁹ In LaNiBN, each orbital occupancy of Ni $3d$ is almost identical to $0.84e$ per spin, resulting in a total of $8.42e$. B $2p$ orbitals have $1.32e$ in total. As observed in the fat bands in Fig. 4, in LaPtBN Pt $5d_{xy}$ and $5d_{z^2}$ orbitals are less filled by $\sim 0.04e$, while the occupancy of Pt $5d_{x^2-y^2}$ increases a little. Compared with LaNiBN, $0.2e$ transfers from the Pt ion to the B $2p$ ion, whereas the occupancies of N $2p$ and La $5d$ remain unchanged. So the Pt ions and the B ions are closer to nominal values of Pt^{2+} and B^{2-} than the Ni and B ions in LaNiBN, indicating less covalent bonding between the Pt and B ions. (Of course, the formal charge concept is murky due to the metallicity and strong hybridization in these systems.) This may be consistent with the longer Pt-B bond length. According to our calculations, however, the occupancies of LaPtBN are nearly unchanged even for the same structure as in LaNiBN, indicating that these distinctions are mainly due to chemical differences between Pt and Ni ions rather than differences in structure.

Since $5d$ systems often show substantial SOC effects, LDA + SOC calculations were performed for LaPtBN. As displayed in the bottom panel of Fig. 4, however, a comparison of the band structures between LDA and LDA + SOC shows negligible SOC effects near E_F , except for a small difference at the Z point. This is due to the wide width of the Pt $5d$ band. Additionally, our calculations substantiated that the EPC strength and, consequently, T_c remain nearly unchanged, when including SOC. As a result, the effects of SOC on the superconductivity of LaPtBN are insignificant. Now, we will exclude the SOC effects.

C. Fermi surface and Fermi velocity

The Fermi surfaces (FSs) of LaNiBN, displayed in Fig. 5(a) and 5(b), consist of three Γ -centered electron surfaces, two M -centered electron surfaces, and a X -centered hole surface. In the Γ -centered FSs, there are cylindrical, dumbbell-like, and ellipsoidal pocket FSs. Here, a tiny Γ -centered ellipsoid is invisible. The cylindrical pocket FS has a mixture of La $5d_{x^2-y^2}$ and Ni d_{z^2} orbitals, while the dumbbell-like one shows La $5d_{x^2-y^2}$ and Ni d_{xy} characters with small B and N $2p$ orbitals. The sandglass-like FS at the M point shows substantial dispersion along the k_z direction and has mainly Ni $3d_{xy}$ and $3d_{z^2}$ characters. The X -centered electron FSs have mainly B $2p$ and N $2p$ characters.

Fig. 5(c) and 5(d) show FSs of LaPtBN, which are similar to those of LaNiBN. However, at the M -centered sandglass-like FS, which is much more dispersive along the k_z direction, the character of Pt $5d$ orbitals mostly

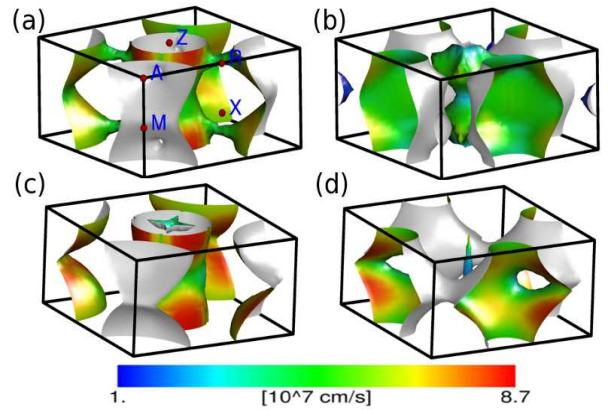


FIG. 5: (Color online) Fermi surfaces (FSs) of (a) and (b) LaNiBN and (c) and (d) LaPtBN in the optimized structure. (For better visualization, FSs of each system are decomposed into two separate plots to reduce the hidden regime.) In both systems, the Γ - and the M -centered FSs possess electrons, but the other ones contain holes. FSs of both systems are similar, but some considerable distinctions appear at the M -point and in the Γ -centered dumbbell-like pockets (see text). The M -centered FSs connect to the Γ -centered large FS in LaNiBN [see (a)], while in LaPtBN the X -centered FSs connect to each other [see (d)]. Fermi velocities are colored dark (blue) for the lowest value and lighter (red) for the highest.

disappears. The Γ -centered cylindrical FS, having mostly Pt $5d_{z^2}$ and La $5d_{x^2-y^2}$ characters with small N $2p$ character, becomes more two-dimensional. A most remarkable distinction appears in the Γ -centered dumbbell FS. The dumbbell substantially reduces to a fishing-bob-like shape, which has mostly Pt $5d_{xy}$ character. The small piece at the M point disappears, but a small Z -centered starfish-like hole pocket appears. Remarkably, although some parts of the Γ -centered FSs are parallel to another part on the $k_z = 0$ plane in both systems, the strong three-dimensionality of the FSs may substantially reduce the strength of nesting, implying no spin or charge-density-wave instability.

To understand the transport properties, we have calculated the FS velocities, as visualized in color in Fig. 5. In the dumbbell and bob FSs, in particular, the FS velocities are low around the Γ point. The cylinders also have low FS velocity along the Γ - M direction. The root-mean-square obtained FS velocities $\langle v_{F,x} \rangle = 3.01$ and $\langle v_{F,z} \rangle = 2.47$ (in units of 10^7 cm/s) for LaNiBN. Compared with the ratio $\langle v_{F,x} \rangle : \langle v_{F,z} \rangle$ of 2:1 in $\text{La}_3\text{Ni}_2\text{B}_2\text{N}_3$,¹⁶ these values are much less anisotropic. The plasma energies are calculated from $\hbar\Omega_{p,ii} = \left[\frac{4\pi e^2 \hbar^2 N(E_F)}{V_c} \langle v_{F,i} v_{F,i} \rangle \right]^{\frac{1}{2}}$, where V_c is the volume of the unit cell. The plasma energies obtained are $\hbar\Omega_{p,xx} = 4.80$ eV and $\hbar\Omega_{p,zz} = 3.95$ eV. LaPtBN is more isotropic, with $\langle v_{F,x} \rangle = 3.50$ and $\langle v_{F,z} \rangle = 3.80$ (in units of 10^7 cm/s). The corresponding plasma energies are $\hbar\Omega_{p,xx} = 4.43$ eV and $\hbar\Omega_{p,zz} = 4.80$ eV. As observed in the electronic structures, these indicate that the transport is three-dimensional in both systems.

TABLE I: Optical phonon frequencies ω (cm^{-1}) at the Γ point. Factor group analysis at the Γ point produces 21 optical modes: 12 Raman active modes of $3A_{1g} + B_{1g} + 4E_g$ and 9 infrared active modes of $3A_{2u} + 3E_u$, where the E_g and E_u modes are two-fold degenerate.^{20,21} Comparison shows remarkable variations in the Pt-related modes. Interestingly, the last four modes have adjacent B and N atoms moving against each other. The atoms in parentheses show relatively small contributions to each mode. The symbol $[110]^*$ indicates a vibration in an inclined direction toward one of the axes in the ab plane.

Symmetry	LaNiBN			LaPtBN		
	ω	Involved atoms	Vibration	ω	Involved atoms	Vibration
E_g	112	La, (B, N)	$[110]$	110	La, (B, N)	$[100], [010]$
E_u	133	Ni, (La, B)	$[110]$	95	La, B, (N)	$[110]^*$
A_{1g}	134	La, (N)	$[001]$	149	La, (B)	$[001]$
A_{2u}	166	Ni, (La, B, N)	$[001]$	141	La, Pt	$[001]$
B_{1g}	194	Ni	$[001]$	50	Pt	$[001]$
E_g	213	Ni, (B, N)	$[110]$	204	Pt, B, N	$[110]^*$
E_g	303	N, (B)	$[110]$	284	N, (B)	$[100], [010]$
E_u	311	N, (B)	$[110]$	283	N, (B)	$[110]^*$
A_{1g}	339	B, N	$[001]$	411	B, N	$[001]$
A_{2u}	366	B, N, (Ni)	$[001]$	406	B, N	$[001]$
E_u	398	B, (N)	$[110]$	436	B, (N)	$[110]^*$
E_g	448	B, (N)	$[110]$	465	B, (N)	$[110]^*$
A_{2u}	938	B, N	$[001]$	992	B, N	$[001]$
A_{1g}	948	B, N	$[001]$	1037	B, N	$[001]$

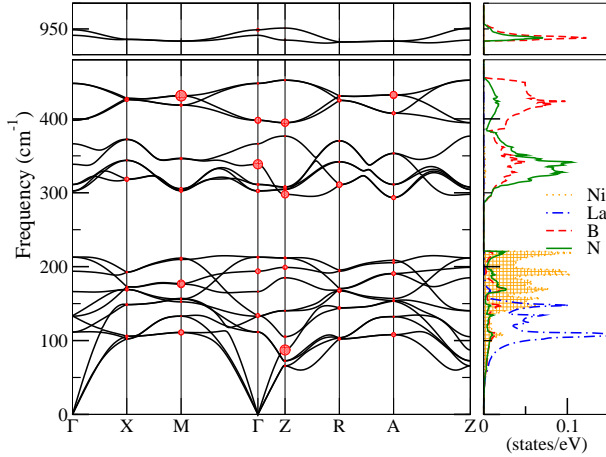


FIG. 6: (Color online) Phonon dispersion and atom-projected phonon DOSs of LaNiBN in the optimized structure. In the phonon spectrum, the size of the red circles is proportional to the partial-mode EPC strength of each phonon mode $\lambda_{\nu,\vec{q}}$, almost uniformly distributed throughout most phonon modes, except for the highest modes.

IV. PHONON DISPERSION AND ELECTRON-PHONON COUPLING

The phonon dispersion curve and the corresponding atom-projected phonon DOSs for LaNiBN are displayed in Fig. 6. The zone-centered phonon modes for both systems are analyzed in Table I. These results are consistent with the frozen phonon calculations of $\text{La}_3\text{Ni}_2\text{B}_2\text{N}$, carried out by Singh and Pickett, who obtained the A_{1g} Raman modes at 106, 323, and 896 (in units of cm^{-1}).¹⁶ Low-energy phonon modes below 220 cm^{-1} come from a

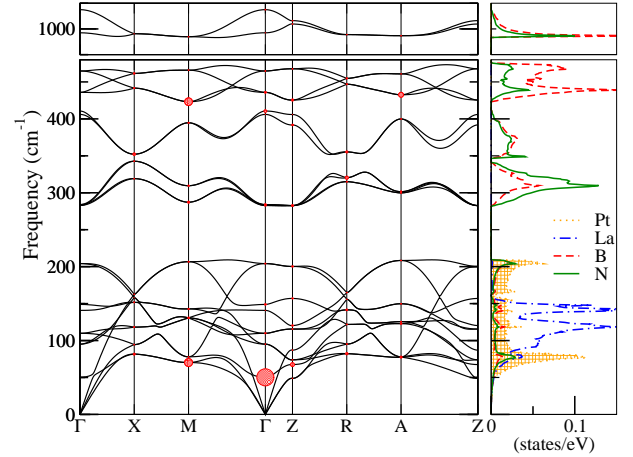


FIG. 7: (Color online) Phonon dispersion and atom-projected phonon DOSs of LaPtBN in the optimized structure. In the phonon spectrum, the size of the red circles representing $\lambda_{\nu,\vec{q}}$ is reduced to half of that of LaNiBN given in Fig. 6 for better visualization. Here, a few modes have relatively large $\lambda_{\nu,\vec{q}}$, though most of all modes involved in EPC (for details, see text).

mixture of vibrations of all atoms, but the Ni character appears mainly in the range of 140 to 220 cm^{-1} . The higher phonon modes originate mostly from the vibrations of B and N ions. The most unusual feature is the isolated modes at about 950 cm^{-1} due to only B and N ions beating against each other, indicating strong B-N bonding along the c axis (see Table I). This value is comparable to the highest B-C bonding stretching mode of $\sim 1200 \text{ cm}^{-1}$ in LiBC,²² though these beating modes do not contribute much to the superconductivity in LaNiBN.

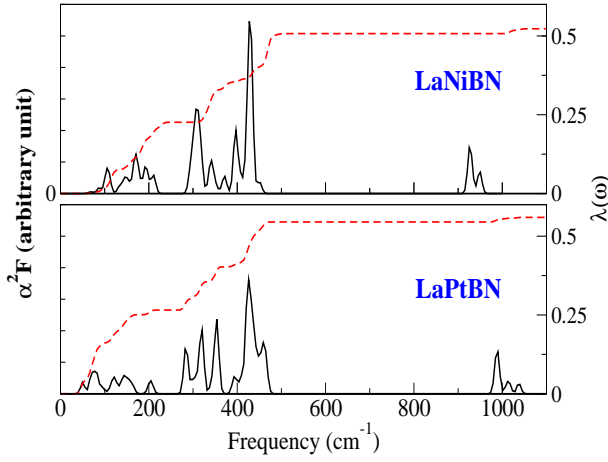


FIG. 8: (Color online) Eliashberg functions (left axis) and frequency-dependent EPC strengths $\lambda(\omega)$ (right axis) of LaNiBN and LaPtBN in the optimized structure. The root-mean-square phonon frequencies $\sqrt{\langle\omega^2\rangle}$ are 184 and 162 K for LaNiBN and LaPtBN, respectively, consistent with slightly stronger EPC in LaPtBN.

Fig. 7 shows the phonon dispersion curve and the atom-projected phonon DOSs of LaPtBN, which are very similar to those of LaNiBN. Remarkably, the main peak of the Pt ion in the phonon DOS shifts down, since a Pt ion is heavier than a Ni ion. As given in Table I, at the zone center the Pt B_{1g} mode has a frequency of 50 cm^{-1} , which is a quarter of that of the Ni B_{1g} mode but is very similar to the frequency of the low-lying in-plane vibrational mode of the Pt ion in SrPt_3P .^{9,23} This mode leads to slightly larger EPC strength in LaPtBN (see below). Additionally, compared with LaNiBN, the frequency of the highest mode is enhanced by about 10%.

Fig. 8 shows the electron-phonon spectral function (Eliashberg function) $\alpha^2 F(\omega)$ and the EPC strength λ together for both systems, which are given by²⁴

$$\alpha^2 F(\omega) = \frac{1}{2N} \sum_{\nu, \vec{q}} \omega_{\nu, \vec{q}} \lambda_{\nu, \vec{q}} \delta(\omega - \omega_{\nu, \vec{q}}), \quad (1)$$

$$\lambda = 2 \int_0^\infty d\omega \frac{\alpha^2 F(\omega)}{\omega} = \frac{N(E_F) \langle I^2 \rangle}{M \langle \omega^2 \rangle}, \quad (2)$$

where $\langle I^2 \rangle$ is the mean-square electron-phonon matrix element averaged over FS and M is the ion mass. λ can also be obtained as an average of $\lambda_{\nu, \vec{q}}$ over N q mesh and all the phonon modes, $\lambda = \frac{1}{N} \sum_{\nu, \vec{q}} \lambda_{\nu, \vec{q}}$. $\lambda_{\nu, \vec{q}}$ are visualized as red circles in Fig. 6 and 7, indicating the mode EPC distributes throughout almost all phonon modes, except for the highest modes, which is consistent with the corresponding Eliashberg functions. (Note that the size of the circles in Fig. 6 is two times larger than in Fig. 7 for better visualization.) Our approach is different from previous studies, which focused on the B A_{1g} mode for $n = 1$ borocarbides and $n = 3$ boronitrides.^{16,25} Our result is in good agreement with the recent experiment using a time-of-flight technique.²⁶ In LaPtBN, a few modes showing

some large $\lambda_{\nu, \vec{q}}$ appear in the B_{1g} mode at the Γ point, in the two fold degenerate modes around 70 and 400 cm^{-1} at the M point, and around 400 cm^{-1} at the A point, but each of these modes equally contributes only 8% to the λ . The two lower energy modes are involved in the Pt vibrations along the c axis, but the other modes are due to the B-N out-of-phase vibrations in the ab plane. In spite of these distinctions, the EPC strengths of the two systems are very close, with $\lambda = 0.52$ and 0.56 for LaNiBN and LaPtBN, respectively. Although the main peaks in $\alpha^2 F(\omega)$ that are mostly attributed to the vibrations of B and N atoms appear in the range of 250 to 500 cm^{-1} , their contributions to λ are only about 50%. The other half is contributed by low-frequency phonon modes below 250 cm^{-1} due to the factor of $\frac{1}{\omega}$ in λ , as shown in Eq. (2). To calculate T_c , we used the Allen-Dynes equation,²⁷ neglecting insignificant strong-coupling corrections in this case,

$$T_c = \frac{\omega_{\log}}{1.2} \exp\left[-\frac{1.04(1 + \lambda)}{\lambda - \mu^* - 0.62\lambda\mu^*}\right], \quad (3)$$

where μ^* is an effective Coulomb repulsion, which is uncertain for these systems but is typically in the range of 0.1 – 0.2. The logarithmically averaged characteristic phonon frequencies ω_{\log} are 376 and 294 K for LaNiBN and LaPtBN, respectively. Thus, $T_c \approx 3.9$ K with $\mu^* = 0.12$ for LaNiBN and 5.4 K with $\mu^* = 0.1$ for LaPtBN, which are very close to the observed values. Considering the similar $N(E_F)$ and larger bandwidth of the Pt $5d$ orbital, these choices of μ^* are reasonable. As a result, the conventional EPC model effectively explains the superconductivity of both systems.

Furthermore, by changing the mass M of the B atom a little, we obtained an isotope shift $\alpha_B = -d(\log T_c)/d(\log M)$ of -0.15 for LaNiBN and 0.13 for LaPtBN, which are similar to the experimentally measured values of 0.1 – 0.25 in a few borocarbides.^{28–30} These values are much smaller than the BCS value of 0.5. This fact is consistent with the fact that the superconductivity is not purely mediated by B-related vibrational modes. The negative isotope shift of B in LaNiBN seems to be unusual but was also suggested through the Raman scattering measurements of the nickel borocarbides.³¹

V. DISCUSSION AND SUMMARY

As a starting point to anticipate the effects of pressure on T_c , we reduced the volume by 3%. (During this reduction, the internal parameters were optimized with the ratio of a/c , fixed to that of the uncompressed structure.) Although the electronic structures in both systems remain nearly unchanged in almost all regimes around E_F , noticeable variations occur in the top of the valence (occupied) bands at the Γ and Z points. In LaNiBN, at the Γ point one of the top valence bands becomes unoccupied, so that the dumbbell FS is nearly separated into two ellipsoids. The phonon frequencies shift up in the phonon

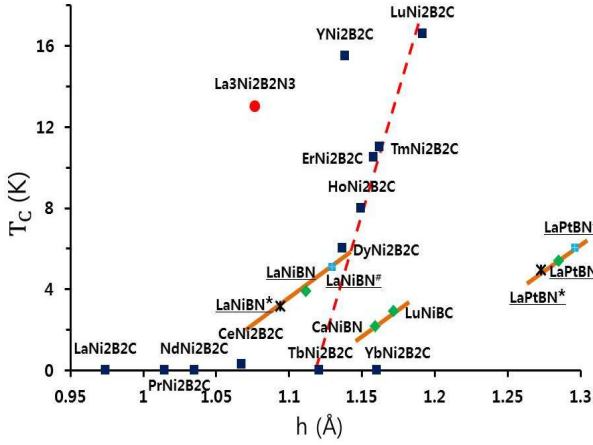


FIG. 9: (Color online) The relation between the superconducting critical temperature T_c and the B height h in the \mathcal{M} -B layer, as displayed in Fig. 1, in borocarbides and boronitrides. Here, $n = 1$ and $n = 2$ systems are denoted by symbols of filled squares and filled diamonds, respectively. The superconducting $n = 1$ borocarbides are connected by the (red) dashed line. The solid lines connect two mutually related compounds in $n = 2$ systems. The data for LaNiBN* (LaPtBN*) and LaNiBN# (LaPtBN#) are obtained from our calculations for 3% compressed and 3% enlarged volumes, respectively. The data are from Ref. [16] for La₃Ni₂B₂N₃, Ref. [33] for YNi₂B₂C, Ref. [34] for LaNi₂B₂C and LuNiBC, Ref. [35] for LuNi₂B₂C, and Ref. [36] for other $n = 1$ borocarbides.

spectrum, indicating the lattice becomes stiffer, as confirmed by enhancing ω_{log} . This leads to decreasing λ and finally reducing T_c by 18%. Changes in LaPtBN are very similar to those in LaNiBN. The flat band along the Γ -Z line is shifted above E_F , so the bob-shaped FS disappears. As expected from the small size of the bob, reduction in T_c of LaPtBN is less significant, only 8%. This may imply less dramatic variation in the superconductivity under pressure in LaPtBN.

A remarkable relation between T_c and the geometric factor has been sometimes observed, *e.g.*, Fe pnictides showing substantial dependence of T_c on the As-Fe-As bond angle.³² Also in the $n = 1$ \mathcal{R} Ni-based borocarbides, a linear dependence of T_c on the ratio of \mathcal{R} -C distance to lattice parameter a was suggested, implying the EPC mediated superconductivity.¹ Interestingly, we found another interesting trend between T_c and the B height h in the \mathcal{M} -B layer, which shows a monotonic increase of T_c with respect to h , as shown in Fig. 9. T_c of $n = 1$

borocarbides shows a very steep slope of $dT_c/dh = 2.27$ K/pm, but no superconductivity has been observed for h below 1.12 Å. One may expect similar behavior for $n = 2$ or $n = 3$ systems, even though the existing data are limited. Using the data for the experimental and $\pm 3\%$ varied volumes for LaNiBN and LaPtBN, we obtained a less rapid increment of T_c with a nearly identical slope of $dT_c/dh = 0.52 (\pm 0.02)$ K/pm. As addressed above in LaNiBN and LaPtBN, different topology and size of one of the Γ -centered FSs among the compounds along each line in Fig. 9 may lead to this change in T_c . These trends suggest that T_c of LaNiBN and LaPtBN could be enhanced by replacing La by a bigger \mathcal{R} atom.

In summary, we have investigated the electronic structures and phonon properties of two superconductors, LaNiBN and LaPtBN, which have structures similar to those of the superconducting Fe pnictides, through first-principles approaches. Our results indicate insignificant effects of SOC, and there is no evidence of magnetic instability in either system. These systems show considerable three-dimensionality with both metallic La-N and \mathcal{M} -B layers, but relatively low DOS at E_F . Both systems have very similar phonon spectra. One remarkable distinction is a significant reduction in the \mathcal{M} B_{1g} mode in LaPtBN, resulting in the enhancement of λ by about 8% compared to the $\lambda = 0.52$ value of LaNiBN. These EPC strengths lead to T_c , consistent with the experimental values. Thus, our findings suggest that the superconductivity is mediated by conventional electron-phonon coupling.

The comparison between our calculated T_c and the experimentally observed value in LaPtBN shows some room, which may be filled by additional interactions like spin fluctuation. However, the rather small contribution of the Pt ion to the DOS near E_F indicates that such a magnetic interaction is improbable in LaPtBN. Further experiments would be desirable to clarify this feature in LaPtBN.

VI. ACKNOWLEDGMENTS

We acknowledge W. E. Pickett and D. J. Scalapino for fruitful discussions and K. Keopernick for providing a program to calculate the Fermi surface and Fermi velocity. This research was supported by the Basic Science Research Program through the NRF of Korea under Grant No. 2012-0002245. C.J.K. and B.I.M. were supported by the NRF under Grant No. 2009-0079947.

* Electronic address: mckwan@korea.ac.kr

¹ For a review, see *Rare earth transition metal borocarbides (nitrides): superconducting, magnetic, and normal state properties*, edited by K.-H. Müller and V. Narozhnyi (Kluwer, Dordrecht, 2001).

² For a review, see I. Askerzade, *Unconventional Superconductors* (Springer, Berlin, 2012), p. 10.

³ N. Imamura, H. Mizoguchi, and H. Hosono, J. Am. Chem. Soc. **134**, 2516 (2012).

⁴ R. J. Cava, H. W. Zandbergen, B. Batlogg, H. Eisaki, H.

- Takagi, J. J. Krajewski, W. F. Peck, Jr., E. M. Gyorgy, and S. Uchida, *Nature (London)* **372**, 245 (1994).
- ⁵ R. J. Keizer, A. de Visser, A. A. Menovsky, J. J. M. Franse, A. Amato, F. N. Gyax, M. Pinkpank, and A. Schenck J. *Phys. Condens. Matter* **11**, 8591 (1999).
 - ⁶ E. Bauer, G. Hilscher, H. Michor, Ch. Paul, E. W. Scheidt, A. Griбанov, Yu. Seropegin, H. Noël, M. Sigrist, and P. Rogl, *Phys. Rev. Lett.* **92**, 027003 (2004).
 - ⁷ K.-W. Lee and W. E. Pickett, *Phys. Rev. B* **72**, 174505 (2005).
 - ⁸ H. Q. Yuan, D. F. Agterberg, N. Hayashi, P. Badica, D. Vandervelde, K. Togano, M. Sigrist, and M. B. Salamon, *Phys. Rev. Lett.* **97**, 017006 (2006).
 - ⁹ C.-J. Kang, K.-H. Ahn, K.-W. Lee, and B. I. Min, *J. Phys. Soc. Jpn.* **82**, 053703 (2013).
 - ¹⁰ N. H. Sung, C. J. Roh, K. S. Kim, and B. K. Cho, *Phys. Rev. B* **86**, 224507 (2012).
 - ¹¹ V. K. Anand, C. Geibel, and Z. Hossain, *Physica C* **460-462**, 636 (2007).
 - ¹² D. J. Singh, W. E. Pickett, H. W. Zandbergen, and R. J. Cava, *Nature (London)* **374**, 682 (1995).
 - ¹³ K. Koepernik and H. Eschrig, *Phys. Rev. B* **59**, 1743 (1999).
 - ¹⁴ J. P. Perdew, K. Burke, and M. Ernzerhof, *Phys. Rev. Lett.* **77**, 3865 (1996).
 - ¹⁵ H. W. Zandbergen, J. Jansen, R. J. Cava, J. J. Krajewski, and W. F. Peck, Jr., *Nature (London)* **372**, 759 (1994).
 - ¹⁶ D. J. Singh and W. E. Pickett, *Phys. Rev. B* **51**, 8668 (1995).
 - ¹⁷ P. Giannozzi et al., *J. Phys. Condens. Matter* **21**, 395502 (2009).
 - ¹⁸ O. Gunnarsson, *J. Phys. F: Metal Phys.* **6**, 587 (1976).
 - ¹⁹ Y. Quan, V. Pardo, and W. E. Pickett, *Phys. Rev. Lett.* **109**, 216401 (2012).
 - ²⁰ H. T. Stokes, D. M. Hatch, and B. J. Campbell, (2007), *ISOTROPY*, 2012, <http://stokes.byu.edu/iso/isotropy.php>.
 - ²¹ E. Kroumova, M. I. Aroyo, J. M. Perez-Mato, A. Kirov, C. Capillasa, S. Ivantcheva, and H. Wondratschek, *Phase Transitions* **76**, 155 (2003); <http://www.crysl.ehu.es/rep/sam.html>.
 - ²² J. M. An, H. Rosner, S. Y. Savrasov, and W. E. Pickett, *Physica B* **328**, 1 (2003).
 - ²³ A. Subedi, L. Ortenzi, and L. Boeri, *Phys. Rev. B* **87**, 144504 (2013).
 - ²⁴ W. L. McMillan, *Phys. Rev.* **167**, 331 (1968).
 - ²⁵ L. F. Mattheiss, T. Siegrist, and R. J. Cava, *Solid State Commun.* **91**, 587 (1994).
 - ²⁶ F. Weber, S. Rosenkranz, L. Pintschovius, J.-P. Castellan, R. Osborn, W. Reichardt, R. Heid, K.-P. Bohnen, E. A. Goremychkin, A. Kreyssig, K. Hradil, and D. L. Abernathy, *Phys. Rev. Lett.* **109**, 057001 (2012).
 - ²⁷ P. B. Allen and R. C. Dynes, *Phys. Rev. B* **12**, 905 (1975).
 - ²⁸ D. D. Lawrie and J. P. Franck, *Physica C* **245**, 159 (1995).
 - ²⁹ K. O. Cheon, I. R. Fisher, and P. C. Canfield, *Physica C* **312**, 35 (1999).
 - ³⁰ H. Hodovanets, S. Ran, P. C. Canfield, and S. L. Bud'ko, *arXiv:1203.4131v2* (2012).
 - ³¹ I.-S. Yang, M. V. Klein, S. Bud'ko, and P. C. Canfield, *J. Phys. Chem. Solids* **63**, 2195 (2002).
 - ³² C.-H. Lee, A. Iyo, H. Eisaki, H. Kito, M. T. Fernandez-Diaz, T. Ito, K. Kihou, H. Matsuhata, M. Braden, and K. Yamada, *J. Phys. Soc. Jpn.* **77**, 083704 (2008).
 - ³³ C. Godart, L. C. Gupta, R. Nagarajan, S. K. Dhar, H. Noel, M. Potel, C. Mazumdar, Z. Hossain, C. Levy-Clement, G. Schiffmacher, B. D. Padalia, and R. Vijayaraghavan, *Phys. Rev. B* **51**, 489 (1995).
 - ³⁴ T. Siegrist, R. J. Cava, J. J. Krajewski, and W. F. Peck, Jr., *J. Alloys Comp.* **216**, 135 (1994).
 - ³⁵ A. L. Ivanovskii, *Russ. Chem. Rev.* **67**, 357 (1998).
 - ³⁶ J. W. Lynn, S. Skanthakumar, Q. Huang, S. K. Sinha, Z. Hossain, L. C. Gupta, R. Nagarajan, and C. Godart, *Phys. Rev. B* **55**, 6584 (1997).